WELDING RESEARCH

SUPPLEMENT TO THE *WELDING JOURNAL*, JUNE 2014
Sponsored by the American Welding Society and the Welding Research Council

Weldability of CMT Joining of AA6061-T6 to Boron Steels with Various Coatings

In this study, the effect of coatings on joining aluminum to steel using a cold metal transfer process was investigated

BY R. CAO, J. H. SUN, J. H. CHEN, AND Pei-Chung WANG

ABSTRACT

The effect of coatings on the weldability of cold metal transfer (CMT) joining of AA6061-T6 to boron steels was investigated. Samples were fabricated and the weld appearance, microstructure, and composition analyses of the joints were examined using scanning electron microscope (SEM), energy-dispersive spectrometer (EDS), X-ray diffraction, and transmission electron microscope (TEM). In addition, the strengths of various joints were evaluated. It was found that molten zinc from a galvanized coating enhanced the molten aluminum filler metal to the wet boron steel substrate, and decreased the heat on the surface of the steel sheet, which made the strength of the joints decrease. The Fe-Zn coating from galvannealed boron steel was not fully molten, and consequently it was of little assistance for the molten aluminum filler metal to wet the boron steel substrate, leading to poor joint quality. Furthermore, sound CMT weld-braze AA6061-T6 to Al-Si coated boron steel and AA6061-T6 to bare boron steel could not be properly produced due to large formation of brittle $FeAl_3$ intermetallic during the welding process.

KEYWORDS

AA6061-T6 • Boron Steels • Coatings • Cold Metal Transfer (CMT) • Weldability • Microstructure • Dissimilar Metals

Introduction

Boron-based hot-forming steels (Ref. 1) and aluminum alloys (Refs. 2–3) have been widely applied for body-in-white construction. Making use of these materials not only reduces vehicle weight, but it also improves crashworthiness and decreases gas emissions (Ref. 4). To prevent surface oxidation of boron steels during warm forming [i.e., 850°C during the forming followed by a cooling rate greater than 50°C/s (Ref. 5)], various coatings have been developed. While the coatings minimize the surface oxidation, their influence on the weldability of boron-based steel is a concern. Since both boron-based steel and aluminum alloy are being applied for structural applications, it is inevitable to encounter the need to join them together.

The joining of aluminum to steel is a great challenge because of the large differences in thermo-physical properties between the two materials and especially the formation of brittle Al-Fe intermetallic compounds (IMCs) at elevated temperatures (Ref. 6). The formation of Fe-Al phases is necessary for achieving an effectual connection between aluminum and steel, but an excessive formation of Fe-Al IMC results in brittleness of the joints (Ref. 7). Thus, in order to suppress the large formation of Fe-Al IMC, solid-state welding methods, e.g., diffusion welding (Ref. 8), explosive welding (Ref. 9), friction welding (Refs. 10–12), and ultrasonic welding (Ref. 13) have been tried to join these dissimilar metals joints. Though the IMC could be hindered using these processes, high efficiency is still lacking, and the shape and size of such solid-state joints are restricted.

Fusion welding processes are feasible to join dissimilar metals with high efficiency (Ref. 14). From the Al-Fe phase diagram (Ref. 15) shown in Fig. 1, Fe-Al IMC could be formed between Al and Fe during the welding process. However, the brittle Fe-Al IMC could be restricted by only melting the aluminum alloy because of the huge difference in melting points of Al (649°C) and iron (1539°C). Gas tungsten arc welding (GTAW)-brazing (Ref. 16) and laser arc welding-brazing (Ref. 17) had been used to connect Al and steel successfully. A fusion welding method with low heat input and high efficiency like cold metal transfer

R. CAO, J. H. SUN, and J. H. CHEN are with Lanzhou University of Technology, Gansu, China. Pei-Chung WANG is with GM Research and Development Center, Warren, Mich.

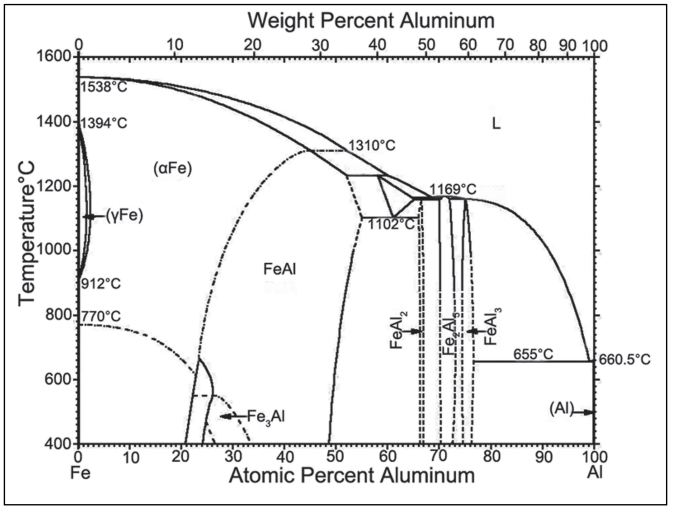

Fig. 1 — Phase diagram of Al-Fe (Ref. 17).

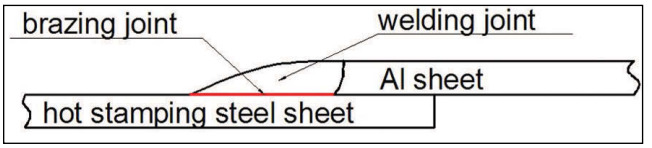

Fig. 2 — Schematic of a CMT weld-braze joint of aluminum 6061-T6 to boron steel.

(CMT) welding-brazing (Ref. 14) might offer a solution for aluminum use in automobile applications. There are many advantages to joining aluminum to steel by the CMT joining technique (Ref. 18). Importantly, the heat input can be controlled, as well as the IMC formation and thickness, thereby enabling optimization of the joint strength.

However, it was unfeasible to join Al and steel with a fusion process without a coating because of a large formation of Fe-Al IMC. The coating has a significant role in the welding of Al and steel. As described earlier, boron steel and aluminum alloys are being widely used in the automotive industry, and various coatings such as Al-Si and Zn were investigated to prevent surface oxidation during the high-temperature process (Ref. 19). Thus, it is inevitable to join aluminum to boron steels with various coatings.

In this study, the effect of coatings on the weldability of CMT joining AA6061-T6 to boron steels was investigated. Weld appearance, microstructure analyses, and tensile-shear strength of the welded joints and joining mechanism at the braze interface were examined and discussed.

Experimental Procedure

Materials

The materials used in the study included 1-mm-thick aluminum AA6061-T6 alloy and 1.5-mm-thick bare, galvanized and galvannealed boron steels. Per our experimental measurements, the compositions of boron steels are shown in Table 1. Al4043 welding wire with a diameter of 1.2 mm was used. Per the manufacturer's datasheet, Table 2 lists the compositions of Al4043 welding wire and AA6061-T6 sheet.

CMT Joining Process

The key feature of the CMT process is the wire motion has been integrated into the joining process and into the overall control of the process. The wire retraction motion assists the droplet detachment during the short circuit, and the metal can transfer into the welding pool without the aid of the electromagnetic force. Thus, there is great control of heat input and weld spatter (Refs. 20, 21).

From the Al-Fe phase diagram (Fig. 1), the melting points of aluminum and iron are 649°C and 1539°C, respectively. This huge difference in melting points makes it difficult to create a metallurgical bond between the aluminum alloy and steel via fusion joining processes without forming intermetallic compounds. One approach to skirt this issue is to control the heat input and keep the steel solid state during the welding process. Therefore, in this study, a weld-braze process was proposed to join aluminum 6061-T6 to boron steels with various coatings.

Figure 2 shows the schematic of a weld-braze joint. As shown, the molten aluminum droplet merged with molten aluminum base metal to form a welded aluminum-to-aluminum connection, whereas, the molten aluminum wire wet the zinc coating on the steel workpiece to form a brazed aluminum-to-steel connection. In order to obtain a weld-braze joint, CMT technology was adopted.

Table 1 — Chemical Compositions of Boron Steels (wt-%)

Materials	C	S	P	Si	Mn	Cr	Ni	Mo	Cu	Nb	V	Ti	Al	N	B	Fe
Galvanized and galvannealed boron steel	0.22	0.002	0.012	0.23	1.15	0.17	0.03	0.001	0.01	0.01	0.004	0.03	0.04	0.007	0.002	Bal.
Bare boron steel	0.14	0.008	0.01	0.23	1.15	0.15	0.05	0.01	0.01	0.01	0.016	0.04	0.06	0.007	0.001	Bal.
Al-Si boron steel	0.24	0.003	0.018	0.26	1.18	0.18	0.03	0.01	0.01	0.01	0.003	0.04	0.13	0.008	0.001	Bal.

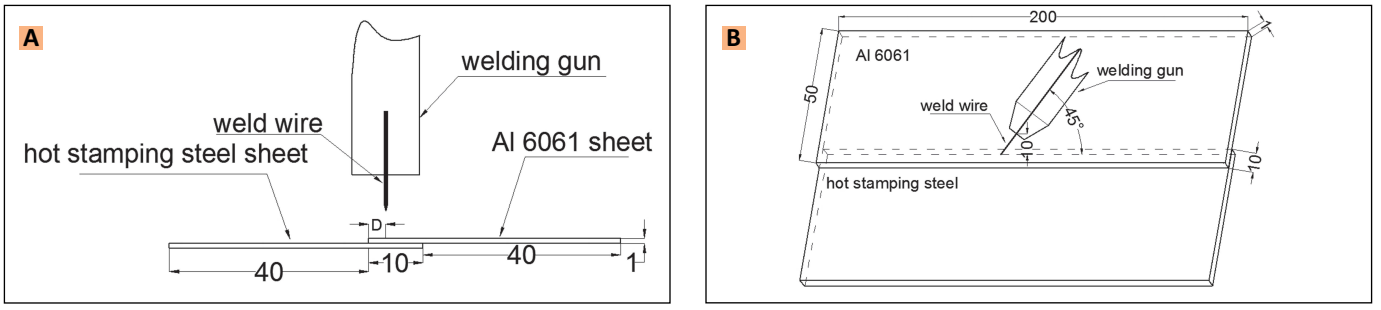

Fig. 3 — Schematic of lapped aluminum-to-steel workpiece. A — Plane; B — side view of the welding gun with respect to the sample.

Sample Fabrication

For the purpose of avoiding the influence of surface contamination, prior to welding the steel sheet was degreased by acetone and tap water. However, to avoid significant porosities produced with the welding process, the Al sheet was degreased by acetone first, and then polished by abrasive cloth, followed by a cleaning with 5–10% NaOH solution at a temperature range of 40° ~ 70°C for 3–7 min and rinsed with tap water. This was followed by surface cleaning with 30% HNO_3 solution at a temperature of 60°C for 1–3 min and then rinsing with tap water.

The lap-shear joint configuration (Fig. 3A) was fabricated from 200 × 50 mm sheets. The arrangement of the test sheets with respect to the welding gun is shown in Fig. 3B. The AA6061-T6 workpiece was placed on top of the steel workpiece in a lap configuration with an overlap distance of 10 mm. The angle between the welding gun and the normal to the lap joint was 45 deg away from the direction of welding. The welding direction was parallel to the lap joint and was offset from the edge of the Al sheet edge by a deviation distance (D). A Fronius arc welding system (CMT 3200) was used to fabricate the samples. The process variables, including the wire feed speed, welding speed, and deviation distance of the wire from the edge of the sheet, were developed during the welding process. A 100% argon shielding gas with a flow rate of 15 L/min was used throughout the experiments.

Analytical Analysis

Standard grinding sample preparation procedures were used and mixed solutions of Nital (i.e., 4 vol-% HNO_3 + 96 vol-% ethanol) were used to etch the samples. The microstructures and compositions of the coatings were observed and analyzed by scanning electron microscope (i.e., SEM 6700F) equipped with energy-dispersive X-ray spectrometer (EDS).

To examine the quality of CMT weld-braze joints, the cross sections of the specimens were prepared and examined. The polished aluminum and steel workpieces were etched by Dix-Keller's. The microstructures and element distributions of the weld were observed and analyzed by SEM equipped with EDS. The phases of the coating and some cracking interfaces were confirmed by XRD (i.e., D8 ADVANCE) transmission electron microscopy (TEM).

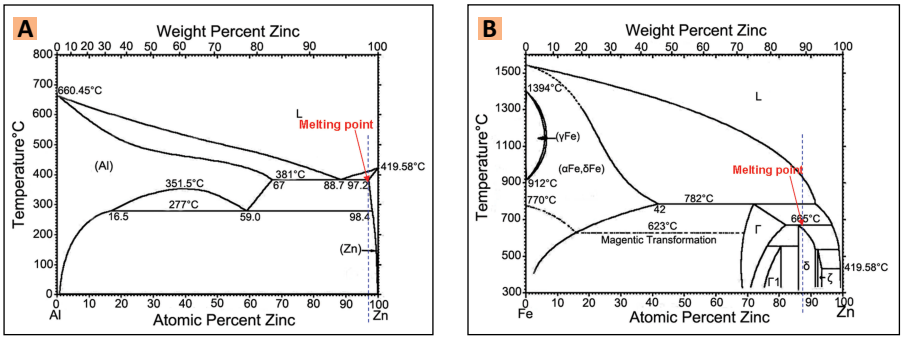

Fig. 4 — Binary phase diagram. A — Al-Zn (Ref. 22); B — Fe-Zn (Ref. 23).

Results and Discussion

Coating Analyses

To analyze the phases of the coatings on three coated hot stamping

Table 2 — Chemical Compositions of AA6061-T6 and Filler Metal (wt-%)

Materials	Si	Fe	Cu	Mn	Mg	Zn	Cr	Ti	Al
Al6061	0.4–0.8	0.70	0.15–0.4	0.15	0.8-1.2	0.25	0.04–0.35	0.15	Bal.
4043 Al wire	4.5–6.0	0.80	0.30	0.05	0.05	0.10	—	0.20	Bal.

Table 3 — Point Analysis Results of Coating of Fe-Zn Galvannealed Boron Steel Shown in Fig. 5A

Location	Al (at.-%)	Fe (at.-%)	Zn (at.-%)	Possible Phase
1	1.4	12.1	86.6	
2	1.1	13.7	85.2	
3	1.1	11.2	87.7	$FeZn_{10}$
4	0.8	12.4	86.7	
Average	1.1	12.4	86.5	

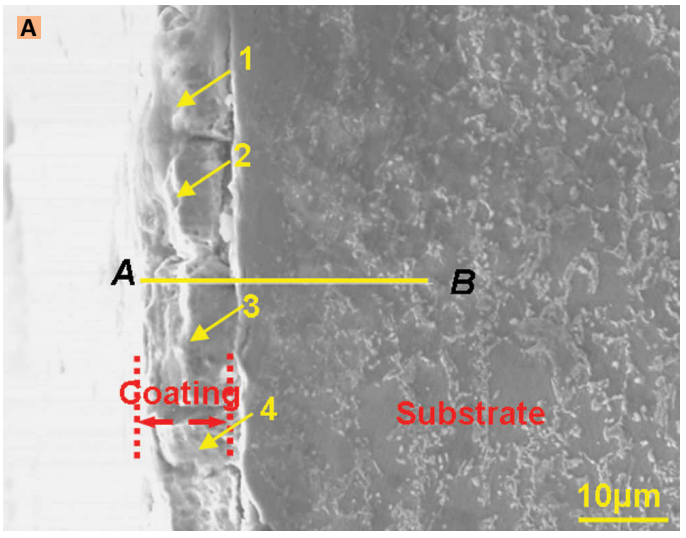

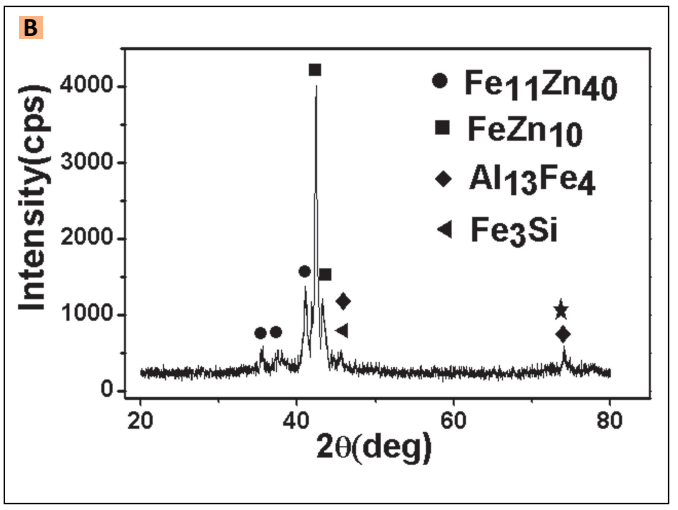

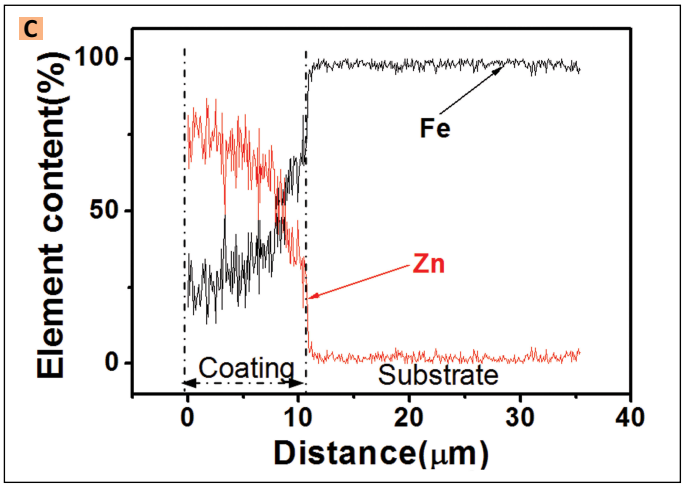

Fig. 5 — Composition analyses of coating layer of galvannealed boron steel. A — Cross section of the coating layer; B — XRD analysis of the coating layer; C — line scanning analysis along line AB shown in Fig. 5A.

steels, Al-Zn, and Fe-Zn (Ref. 22) phase diagrams presented in Fig. 4A and B, respectively, were referenced. For the Al-Zn phase diagram, the phases at room temperature were composed of Al-Zn eutectoid, Zn solid solution, and Al solid solution. However, for the Fe-Zn phase diagram shown in Fig. 4B, phases at room temperature consisted of several intermetallic phases, such as Γ (Fe_3Zn_{10}), Γ1 (Fe_5Zn_{21}), δ ($FeZn_{10}$) and ζ ($FeZn_{13}$) (Ref. 23).

Composition analyses of coating layers for galvannealed boron steel, galvanized boron steel, and Al-Si-coated boron steel are shown in Figs. 5–7, respectively. As shown in Fig. 5, cross-section examination of galvannealed boron steel was conducted and the results presented that a coating with a thickness of ~10 mm (Fig. 5A) was formed. X-ray diffraction analyses of the coating shown in Fig. 5B and C indicated it was mainly composed of Fe-Zn IMC. By combining Fe-Zn binary phase diagram shown in Fig. 4B and EDS analysis results of the coating shown in Table 3, it was found that the δ-$FeZn_{10}$ phase was formed when Fe and Zn contents reached respectively ~12% and ~87%. These results suggested that the coating layer for galvannealed boron steel was primarily composed of δ-$FeZn_{10}$ phase.

The thickness and compositions of galvanized coating on boron steel were examined and analyzed, and the results are shown in Fig. 6A, B, and C. As shown in Fig. 6A, the zinc coating layer had a thickness of ~10 mm. By combining the results shown in Figs. 6B, C, 4A, and Table 4, it was found that when the Al and Zn contents reached ~2–3% and ~96–98%, respectively, Zn solid solutions were formed, which suggested that the coating of galvanized boron steel was mainly composed of Zn solid solutions. Furthermore, line scan analysis results shown in Fig. 6C revealed that an Al-rich phase was formed at the interface between the coating and steel. These results indicated that the microstructure adjacent to the interface consisted of not only Zn but ultrathin Fe-Al IMC due to the hot-dip galvanizing process, which was consistent with the results found in Ref. 24.

Figure 7 presented the cross section and compositions of Al-Si-coated boron steel. Careful examination of the results shown in Fig. 7A showed that the coating layer had a thickness of ~35 mm. By combination of the results shown in Fig. 7B, C, and Table 5, it was found that the coating was primarily composed of two layers. The external dark reaction layer A, shown in Fig. 7A, mainly consisted of $FeAl_3$ IMC, and the bright layer B next to the base metal mainly consisted of AlFeSi IMC. x-ray diffraction analysis results of the coating shown in Fig.7B further revealed that the coating of Al-Si boron steel was composed of series Fe-Al and Fe-Al-Si IMC. The weldability of the Al-Si boron steel and aluminum sheets are discussed in the next section.

Joining AA6061-T6 to Boron Steel

To assess the effect of coating on the weldability, weld appearance of weld-braze AA6061-T6 to boron steel was examined first. Figure 8 shows the weld appearance of CMT weld-braze 1.0-mm-thick AA6061-T6 to 1.5-mm-thick bare boron steel. As shown, while the weld metal barely covered the aluminum substrate, it fully spread on the steel substrate. This was primarily attributed

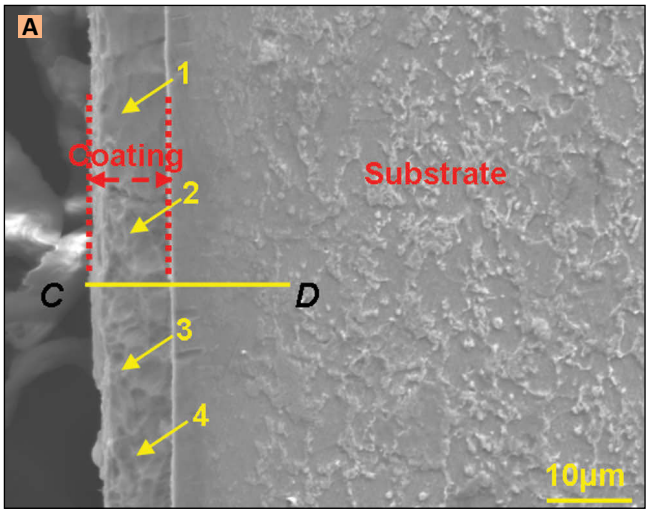

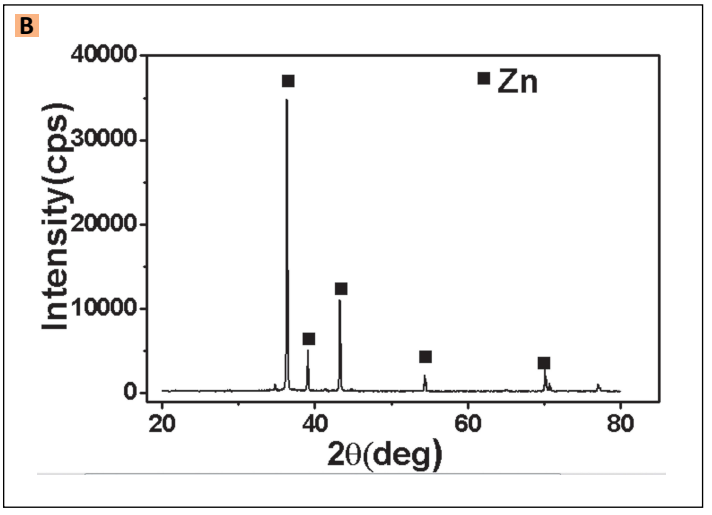

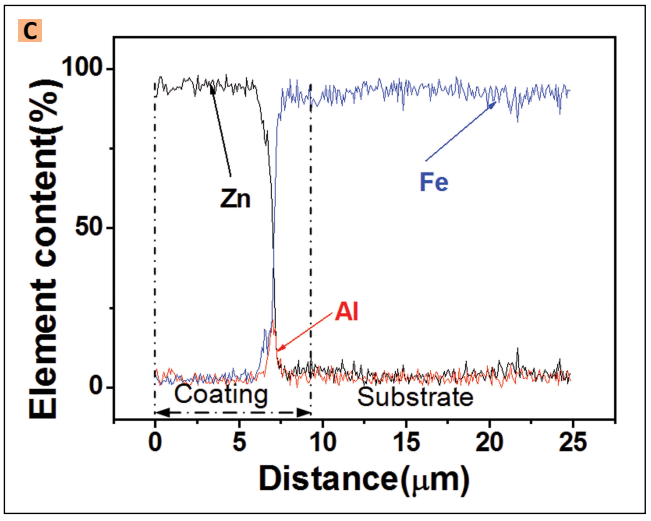

Fig. 6 — Composition analyses of coating layer of galvanized boron steel. A — Cross section of the coating layer; B — XRD analysis of the coating layer; C — line scanning analysis along line CD shown in A.

to the combination of the strong affinity of aluminum to steel and melting of the aluminum substrate. Because enthalpy of mixing of aluminum in iron (i.e., –48 kJ/mole) was less than that of aluminum in aluminum (i.e., 0 kJ/mole), affinity of aluminum in aluminum was weaker than that of Al in Fe (Ref. 25). Therefore, the molten aluminum spread to the steel side rather than the aluminum side during welding.

The microstructural variations at the interface and weld metal of CMT joined AA6061-T6 to boron steel are shown in Fig. 9. From the cross section shown in Fig. 9A, the weld metal was separated from the base metal. Moreover, a significant amount of the cracks were observed in the weld metal. Energy-dispersive spectrometer analysis of the region A shown in Fig. 9A was performed and the results are listed in Table 6. As presented in Table 6 and Fig. 9B, massive brittle $FeAl_3$ IMC at the location 1 was distributed among α-Al solid solutions (in Region 2) and Al-Si eutectic (in Region 3) in the weld metal. Furthermore, experimental observations showed that a significant amount of the boron steel was molten under an intensive arc heat. The molten steel reacted with aluminum filler metal, leading to formation of a large amount of brittle Fe-Al IMC. These results suggested that the cracks observed in the weld metal likely resulted from the combination of the formation of brittle Fe-Al IMC and thermal-induced residual stresses due to the difference in coefficient of thermal expansion between steel and aluminum. Figure 9C shows the cracking interface shown in Fig. 9A between the weld metal and bare steel sheet. In addition, EDS analysis of locations 4 and 5 shown in Fig. 9C and XRD analysis at the cracking interface between the weld metal and steel sheet were performed. The XRD results are shown in Fig. 9D. These results indicated that massive brittle Fe-Al IMC existed at the cracking interface. Thus, sound joints between AA6061-T6 and bare boron steel could not be formed by the CMT method.

Table 4 — Point Analysis of Coating Layer of Galvanized Coated Boron Steel Shown in Fig. 6A

Location	Al (at.-%)	Zn (at.-%)	Possible Phase
1	3.2	96.8	
2	2.3	97.7	
3	2.4	97.6	Zn solid solutions
4	2.9	97.1	
Average	2.7	97.3	

Joining AA6061-T6 to Al-Si-Coated Boron Steel

To sustain the temperature in the range of 950°C during hot stamping, Al-Si-coated boron steel was developed for automotive applications (Ref. 26). To examine if Al-Si coating would affect the weldability, CMT joining AA6061-T6 to Al-Si-coated boron steel was conducted. Figure 10 shows the appearances of the welds. Experimental observations revealed that the welds split immediately after welding. Figure 10A and B shows the weld appearance of the Al and steel sheet

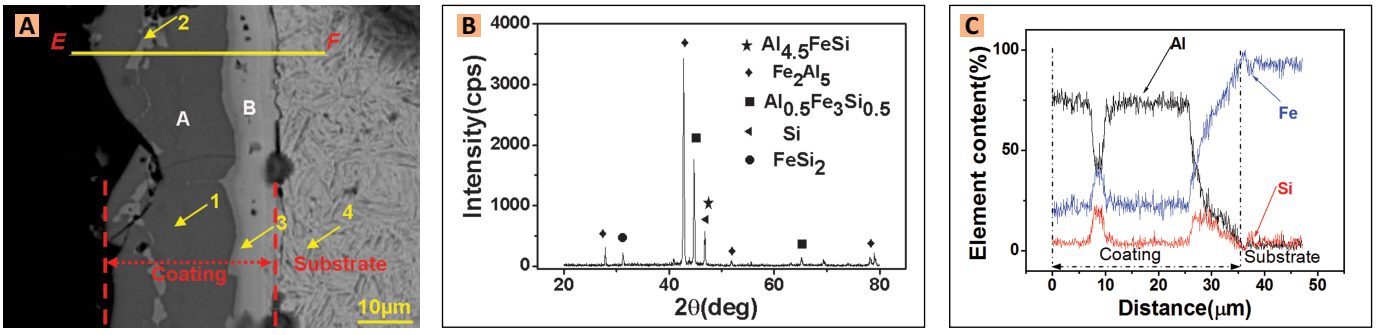

Fig. 7 — Composition analysis of coating layer of Al-Si boron steel. A — Cross section; B — XRD analysis; C — line scanning analysis along line EF shown in A.

Fig. 8 — Weld appearance of CMT for 1-mm-thick AA6061-T6 to 1.5-mm-thick bare boron steel.

sides, respectively. Careful examinations of the welded specimens indicated that the poor weld quality was likely caused by the formation of brittle Fe-Al and Fe-Al-Si IMC, shown in Fig.7B and C, and thermal residual stresses developed during the welding.

To validate this observation, the compositions and phases of the weld metal and the cracking interface were analyzed, and the results are shown in Fig. 11 and Table 7. As shown, coarse columnar grains with cracks (zone A in Fig. 11A) and equiaxed crystal grains (zone B) were observed at the upper and lower parts of the weld metal, respectively. The weld metal shown in Fig. 11A mainly consisted of two different features, i.e., dark and bright regions. The compositions of the dark region (location 1) of the weld metal shown in Table 7 were 96.4 at.-% Al, 2.4 at.-% Fe, and 1.2 at.-% Si, which indicated the phases of this weld metal were αa-Al, and some Al-Si eutectic phases (location 2) distributed among the α-Al base metal. The compositions of the bright region (location 3) of the weld metal shown in Table 7 are 67.7 at.-% Al, 31 at.-% Fe, and 1.3 at.-% Si, which suggested the phases of this weld metal were primarily $FeAl_3$ IMC. In addition, there existed a transition zone between the dark and bright regions. EDS analysis results showed that the phase of this zone (location 4) was $FeAl_3$ IMC, too. To further confirm the phases of the cracking interface shown in Fig. 11A, corresponded EDS analysis of locations 5 and 6, shown in Fig. 11D, on the cracking interface and XRD analysis of the cracking interface were performed and the results are shown in Table 7 and Fig. 11E, respectively. The results shown in Fig. 11D and E revealed that a significant amount of brittle Fe-Al IMC existed at the cracking interface (Fig. 11A and D) between the weld metal and Al-Si boron sheet. From these analyses, we concluded that Al-Si-coated boron steel could not be properly joined to AA6061-T6 primarily due to formation of large amounts of brittle $FeAl_3$ IMC.

Table 5 — Point Analysis Results of Coating Layer of Al-Si Coated Boron Steel Shown in Fig. 7A

Location	Al (at.-%)	Si (at.-%)	Fe (at.-%)	Possible Phase
1	72.24	2.60	25.16	$FeAl_3$
2	44.38	16.16	39.47	AlFeSi
3	19.92	5.44	74.65	Fe_3Al
4	0	0	100	***α-Fe***

Table 6 — EDS Analysis Results of Zones 1 – 5 in Fig. 9

Location	Al (at.-%)	Si (at.-%)	Fe (at.-%)	Possible Phase
1	77.43	1.17	21.40	$FeAl_3$
2	83.78	16.22	0	Al-Si eutectic
3	98.3	1.4	0.47	α-Al
4	28.8	3.2	67.9	$FeAl_3$
5	29.6	3.4	67.0	$FeAl_3$

Joining AA6061-T6 to Galvannealed Boron Steel

Figure 12 shows the effect of wire feed speed on the appearance of CMT weld for 1.0-mm-thick AA6061T6 to 1.5-mm-thick galvannealed boron steel. Tests were conducted with a wire feed speed of 3 m/min and the results shown in Fig. 12A indicated that filler metal still could not properly wet the steel surface, and consequently the narrow weld was formed. With an increase of wire feed speed from 3 to 4.5 m/min, the weld became discontinuous and sporadic. Then, the surfacing welds were trialed on the surface of galvannealed boron steel with wire feed speeds of 4 and 5 m/min. As shown in Fig. 12C, the molten aluminum also didn't wet the steel substrates well, which is the rea-

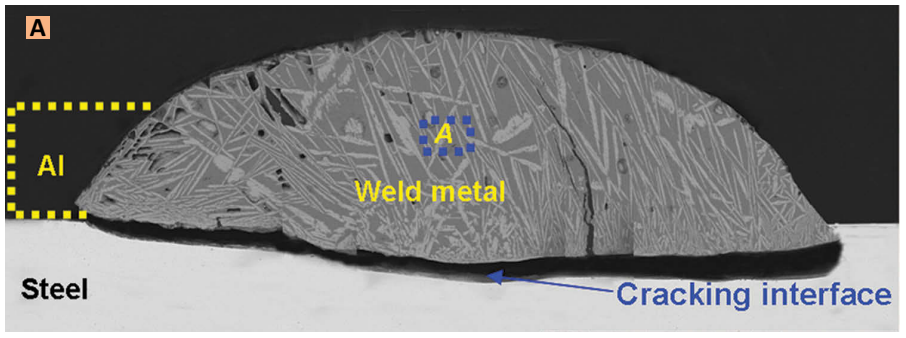

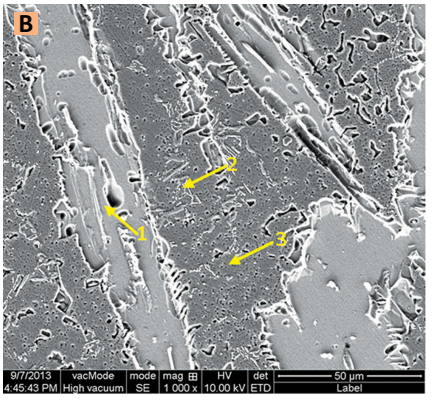

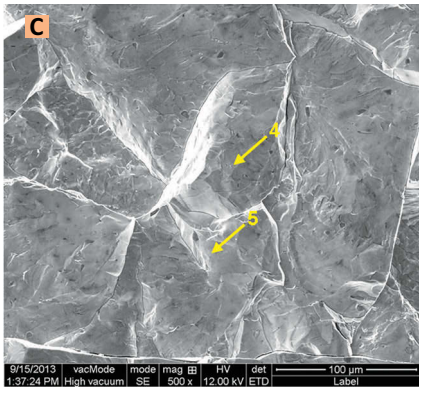

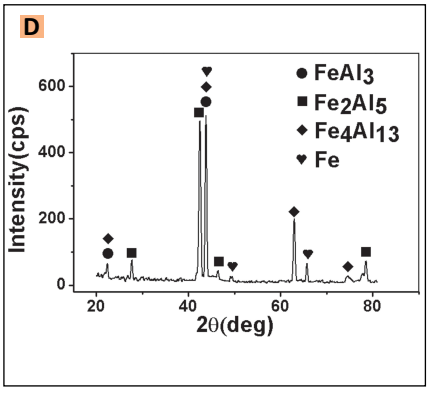

Fig. 9 — A — Cross section of CMT weld for 1.0-mm-thick AA6061-T6 to 1.5-mm-thick bare boron steel; B — enlarged view of zone A shown in A; C — crack interface shown in A between the weld metal and bare steel sheet; D — XRD analysis at the crack interface shown in A between the weld metal and steel sheet.

son for the poor appearance of CMT welded AA6061T6 to galvannealed boron steel. Experimental observations indicated that the arc was unstable and large spatter occurred during CMT joining. Joining mechanisms of the joints are discussed next.

Before the process optimization tests were performed, we examined the cross-section, microstructure, and line scan analysis of CMT welded lap AA6061-T6 to galvannealed boron steel joints, and the results are shown in Fig. 13. As shown in Fig. 13A, the molten filler metal was deposited on the surface of the steel substrate with a poor contact angle of ~115 deg. From Fig. 13A, three different zones (i.e., Zones A, B, and C) were observed at the interface between the weld metal and galvannealed boron steel. EDS analyses of locations 1 to 2 in Zone A shown in Fig. 13B, locations 3 to 5 in Zone B shown in Fig. 13D, and locations 6 to 7 in Zone C shown in Fig. 13F were conducted, and the results are shown in Table 8. As presented in Fig. 13B and Table 8, at the Zone A of bonding interface between the weld metal and galvannealed boron steel consisted of Fe_3Al and $FeAl_3$ IMC with a thickness of ~5 μm. EDS results showed that reaction layer of Zone B shown in Fig. 13D was mainly composed of Zn, Al, and Fe. The aluminum element in the molten weld metal interacted with Fe-Zn coating, and consequently, an interface layer consisted of Fe_2Al_5, Fe_4Al_{13}, α-Al and α-Zn was produced during the welding process. At the Zone C in Fig. 13A, severe cracks were observed between the weld metal and galvannealed boron steel. Especially for enlarged Zone C in Fig. 13G, the interface near the steel is mainly composed of $FeZn_{10}$ compound, which is consistent with the phase in the coating layer in Fig. 5. Therefore, these results showed that the galvannealed coating was not fully molten so that molten aluminum hardly wetted the steel substrates at this zone, and consequently sound CMT welding of AA6061-T6 and galvannealed boron steel could not be attained.

Table 7 — EDS Analysis Results of Zones 1–6 in Fig. 11

Location	Al (at.-%)	Si (at.-%)	Fe (at.-%)	Possible Phase
1	96.4	1.2	2.4	α-Al
2	90.2	9.3	0.5	α-Al + Al-Si eutectic
3	67.7	1.3	31	$FeAl_3$
4	66.8	6.4	26.8	$FeAl_3$
5	65.1	33.6	1.7	$FeAl_3$
6	53.8	37.5	8.7	Si-rich $FeAl_3$

Joining AA6061-T6 to Galvanized Boron Steel

After we had examined the Al-Si-coated and galvannealed boron steel, CMT joining of AA6061-T6 to galvanized boron steel was also performed. Figure 14A presents the appearances of the welds. As shown, welds with low reinforcement were produced. Experimental observations showed that adequate wetting of the molten filler metal on the substrates and a stable arc were observed. To understand the effect of galvanized coating on the weldability, the cross section of CMT welded AA6061-T6 to galvanized boron steel was examined, and the results are shown in Fig. 14B. A welded connection was developed between the molten filler metal and aluminum substrate on one side, while a brazed connection was formed

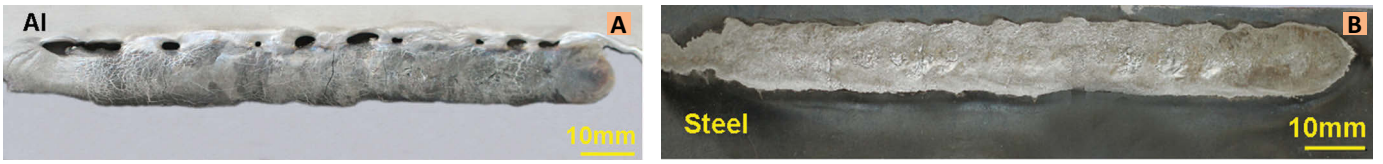

Fig. 10 — Weld appearance of CMT weld-braze of 1.0-mm thick AA6061-T6 to 1.5-mm thick Al-Si boron steel with a wire feed speed of 4.5 m/min. A — Weld surface at Al sheet side; B — detached surface of weld from Al-Si-coated boron steel sheet side.

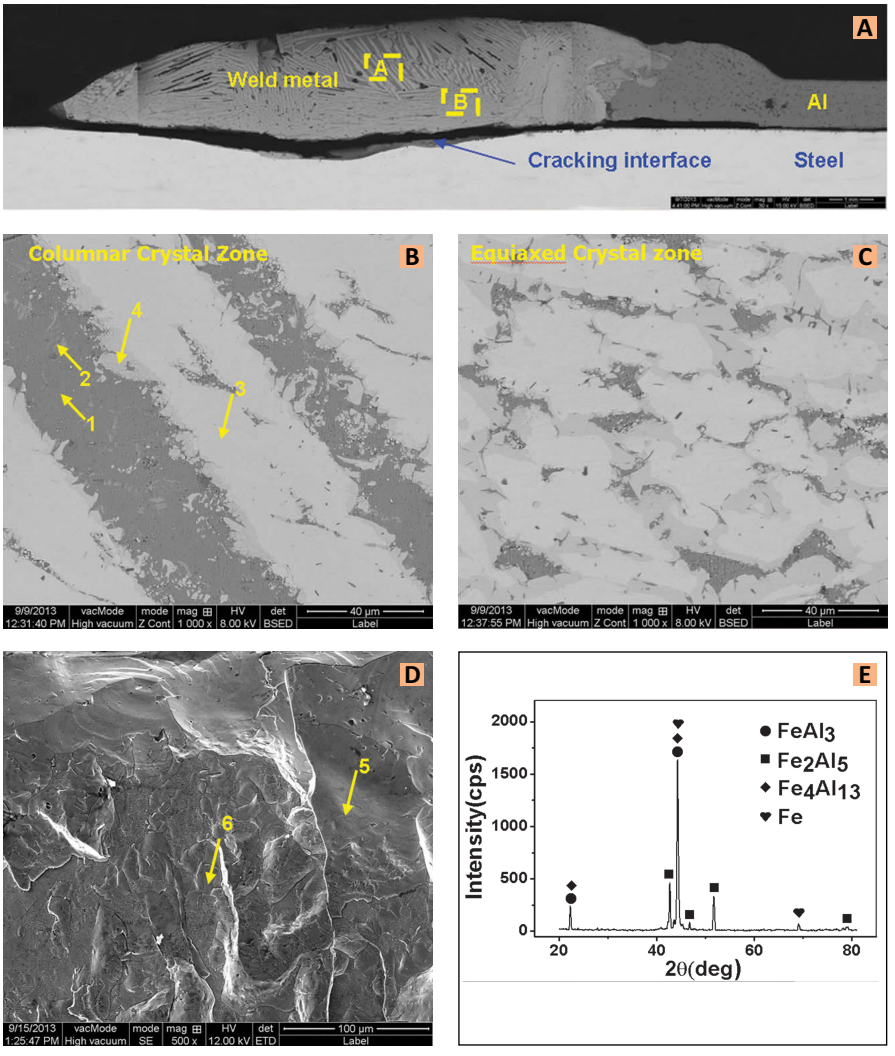

Fig. 11 — CMT weld of AA6061-T6 to Al-Si boron steel. A — Weld metal; B — enlarged view of zone A in A; C — enlarged view of zone B in A; D — cracking interface (shown in Fig. 11A) between the weld metal and Al-Si boron sheet; E — XRD analysis at the cracking interface shown in Fig. 11D.

between the aluminum and steel. The reaction products along the brazing interface can be divided into two zones: zinc-rich Zone A and Fe-Al reaction layer B. Figure 15 shows the corresponding SEM micrographs of these two zones. The phases of these zones were determined by EDS, and the results are shown in Table 9.

Microscopy analyses revealed that the Zn element at the Zone A (i.e., the toe of a lap weld observed in Fig. 15A and B) had been driven from the steel surface toward the regions near the weld toe. EDS analysis of regions 1 and 2 in Zone A were performed, and the results listed in Table 9 indicated that they were mainly composed of bright dendrites of Al-Zn eutectoid and α-Al. Region 1 had a zinc content of 22.4%, which corresponds to the chemical compositions of the eutectoid fcc-Al + hcp-Zn (Ref. 27). In addition, the gray zone (Region 2), which mainly consisted of α-Al existed between the grey dendrites of Al-Zn eutectoid. Furthermore, some Si granules observed at Region 3 existed among the Al-Zn eutectoid and αa-Al. The Zn element was known to enhance the wetting of the molten aluminum alloy and filler metal on the steel substrate (Ref. 28). Compared to Fe, aluminum has a larger affinity to Zn (Ref. 29), and consequently, Al-Zn phases were favored than the Fe-Al IMC, which is the reason why most Al-Zn eutectoid phases were formed in Zone A.

At the brazing interface (i.e., Zone B), the interfacial microstructure shown in Fig. 15C was found to be homogeneous and had a continuous morphology with a thickness of 2–5 μm. The thickness of the reaction layer was reduced greatly because of the Zn evaporation from the arc heat (Ref. 14). To identify the elements, distribution at the brazing layer, EDS line scanning of the middle interface B was carried out and the results are plotted in Fig. 15 D. As observed, the Fe element content decreased whereas the Al element content increased along the interface. In general, it was found that the distribution ratio of Fe/Al remained unchanged at the Fe-Al reaction layer, which indicated that IMC were likely formed in another way.

The EDS analyses at the Zones 4 and 5 of the interface were performed, and the results are shown in Table 9. As shown, the phase (denoted by Zone 4) near the steel substrate consisted of 38.7 at.-% Al, 60.7 at.-% Fe, and 1.2 at.-% Si, while the phase (denoted by Zone 5) near the weld metal contained 72.2 at.-% Al, 23.9 at.-% Fe, and 3.9 at.-% Si, which showed that the possible phases at the brazing interface were Fe_4Al_{13} and Fe_2Al_5 IMC. To fur-

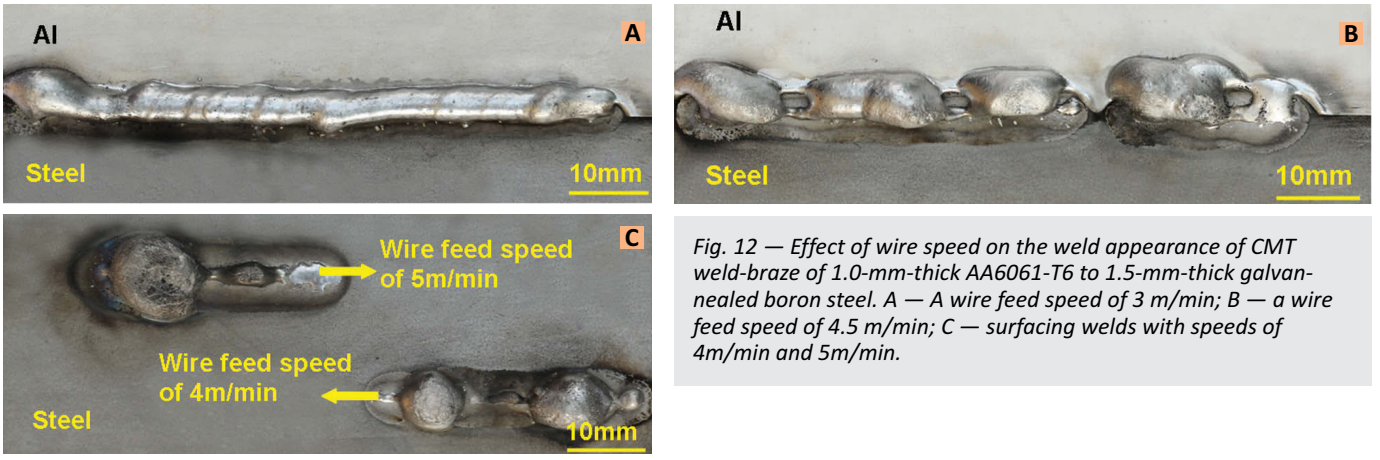

Fig. 12 — Effect of wire speed on the weld appearance of CMT weld-braze of 1.0-mm-thick AA6061-T6 to 1.5-mm-thick galvannealed boron steel. A — A wire feed speed of 3 m/min; B — a wire feed speed of 4.5 m/min; C — surfacing welds with speeds of 4m/min and 5m/min.

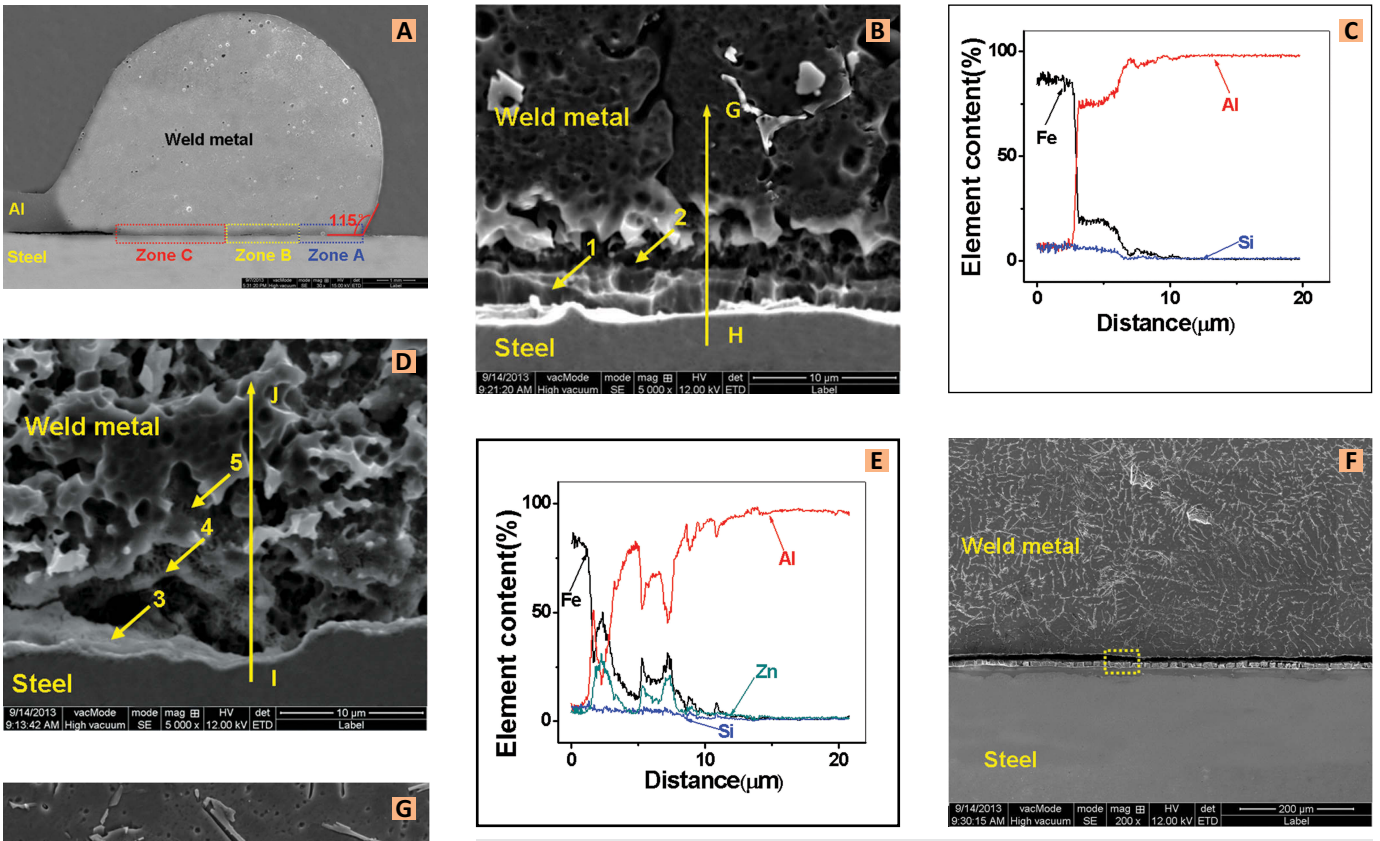

Fig. 13 — CMT weld of 1.0-mm-thick AA6061-T6 to 1.5-mm-thick galvannealed boron steel. A — Cross section; B — microstructure of zone A; C — line scan along yellow HG at interface of Zone A; D — microstructure of zone B; E — line scan along yellow IJ at interface of Zone B; F — microstructure of Zone C; G — enlarged Zone C.

ther confirm Fe-Al IMC phases at the brazing interface, TEM micrograph and selected area diffraction patterns (SADP) corresponding to the specific regions at the brazing interface were prepared, and the results are shown in Fig. 16.

As shown, the intermetallic layer at the steel/weld metal interface contained the grains with different morphologies. The finger-like grains, which were approximately perpendicular to the interface, were formed near the steel matrix, and trapezoidal grains were produced next to the weld metal. Electron diffraction patterns performed on the finger-like grains of region B confirmed them to be Fe_2Al_5 phase. The trapezoidal grains of region A located between the grains and weld metal were identified as Fe_4Al_{13} phase. In addition, massive dislocations were observed in Fe_2Al_5 phase, which might

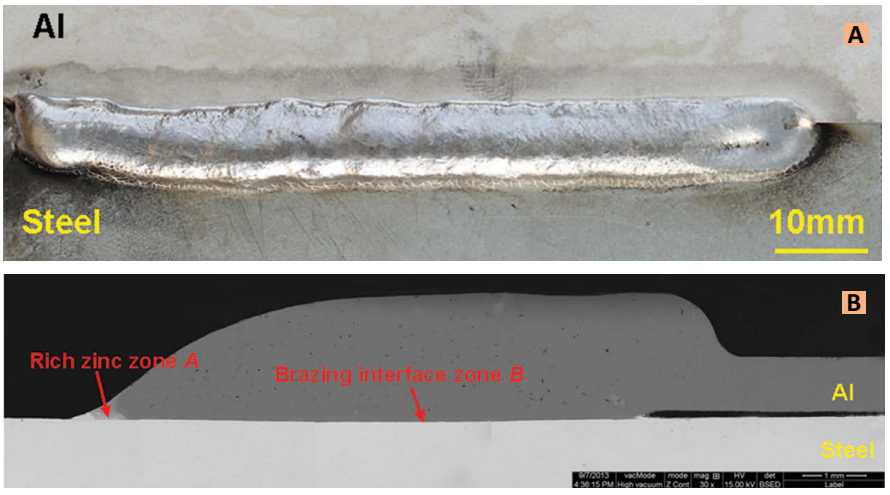

Fig. 14 — CMT weld of 1.0-mm-thick Al to 1.5-mm-thick galvanized boron steel under a wire feed of 4.5 m/min. A — Weld appearance; B — cross section.

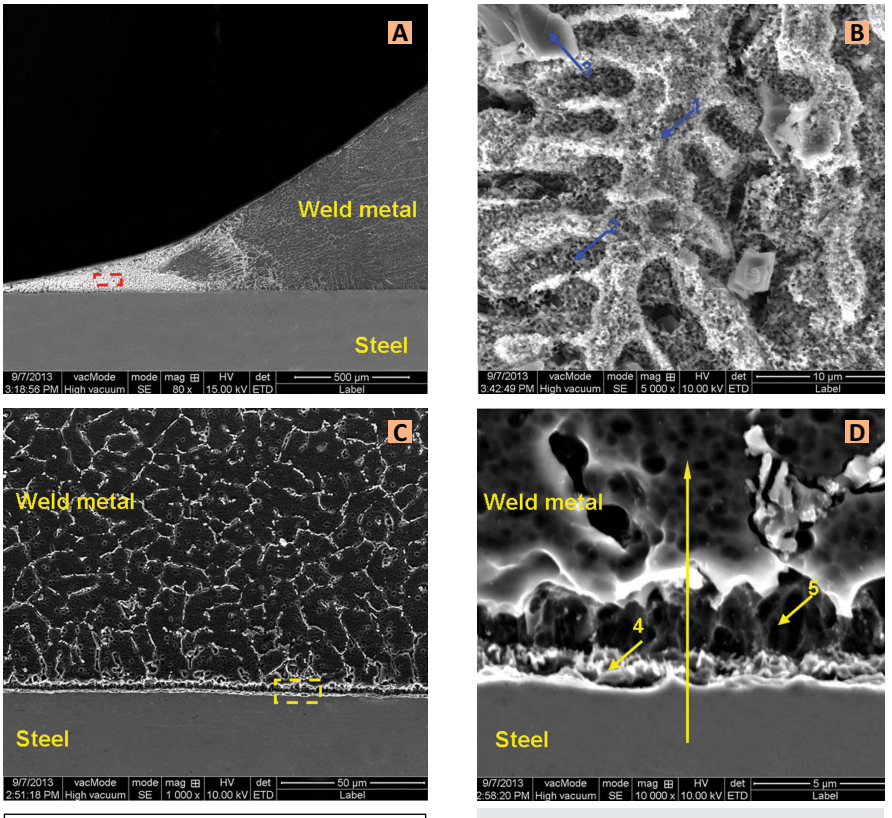

Fig. 15 — Microstructures of CMT weld-braze of 1.0-mm-thick AA6061-T6 to 1.5-mm-thick galvanized boron steel. A — Zone A; B — enlarged Zone A; C — braze interface B; D — enlarged zone B; E — line scan at the brazing interface B.

have nucleated from the phase boundaries and prolonged with the growth of the finger-like Fe_2Al_5 grains. From the aforementioned analyses, the thickness of brittle brazing layer is smaller than the critical thickness of 10 μm (Ref. 30), and this contributed the formation of a sound AA6061-T6 to galvanized boron steel weld.

To evaluate the strength of CMT weld-braze AA6061-T6-galvanized boron steel, quasistatic tests were conducted, and the results are shown in Fig. 17. The joint strength was defined as the failure load/specimen width, N/mm. For the purpose of comparison, the results of CMT welded AA6061-T6 to bare boron steel, Al-Si-coated steel and galvannealed steel with the same dimensions were also included in Fig. 17. As shown, the strengths for both AA6061-T6 to bare boron steel and Al-Si-coated steel joints were relatively low due to massive formation of brittle Fe-Al IMCs during the welding process, and the strength for AA6061-T6 to galvannealed steel was also relatively weak because of the poor bond formed at the brazing interface. However, for CMT weld-braze AA6061-T6 galvanized boron steel, the strength was sound (i.e., 208 N/mm), and the failure location for this joint was at the aluminum heat-affected zone shown in Fig. 18, which indicated that sound CMT weld-braze AA6061-T6 galvanized boron steel joints were produced.

Weldability of CMT Joining AA6061-T6 to Boron Steel

The aforementioned test results and analyses showed that galvanized boron steel was joined successfully to AA6061-T6 by the CMT process using $AlSi_5$ feed wire, while the weldability of AA6061-T6 to bare boron steel, AA6061-T6 to Al-Si-coated boron steel, and AA6061-T6 to galvannealed boron steel was poor. From the point analysis results of the coating layer shown in Tables 3 and 4, Fe-Zn and pure Zn coatings on galvannealed and galvanized boron steels contained about 86% and 96% Zn element, respectively. Refer to Fig. 4 (i.e., Al-Zn and Fe-Zn binary phase diagrams), the melting points of pure Zn and Fe-Zn coatings were 381°C and 665°C, respectively. Pure Zn coating was readily molten under the CMT arc, and molten filler metal spread on the liquid zinc layer other than the surface of the solid steel substrate, which improved the wettability and spreadability of the molten weld metal. In addi-

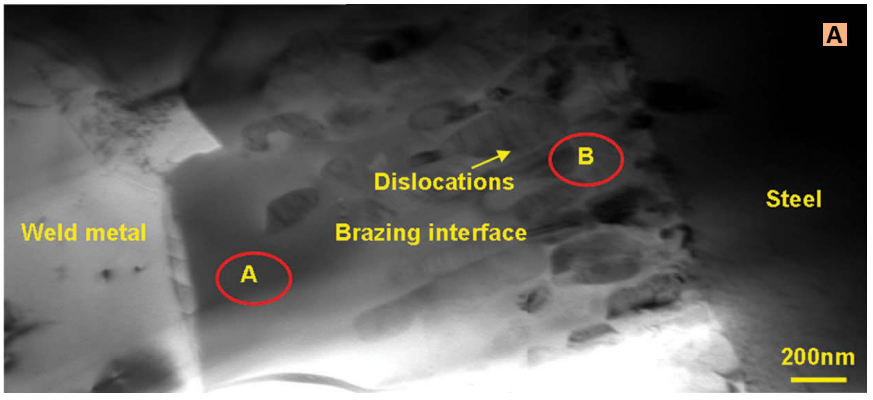

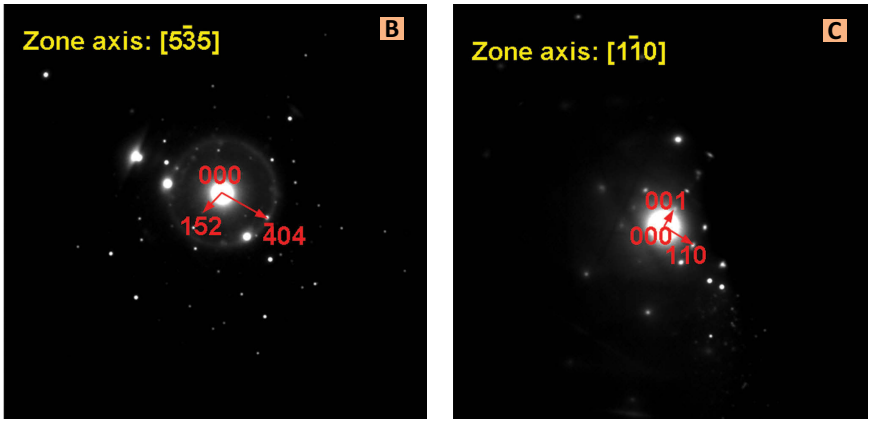

Fig. 16 — TEM micrograph and indexed selected area diffraction patterns at the braze interface. A — Morphology of grains present at IMC resolved in TEM model; B — SAD corresponding to region A; C — SADP corresponding to region A.

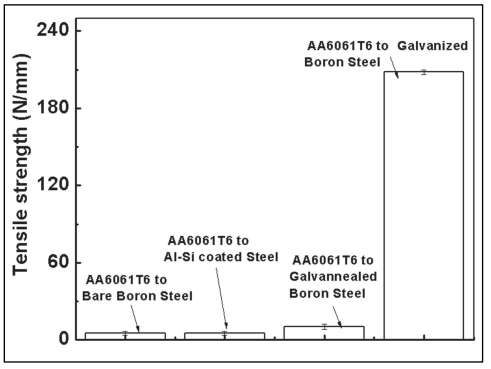

Fig. 17 — Tensile strengths of CMT joining of AA6061-T6 to boron steel.

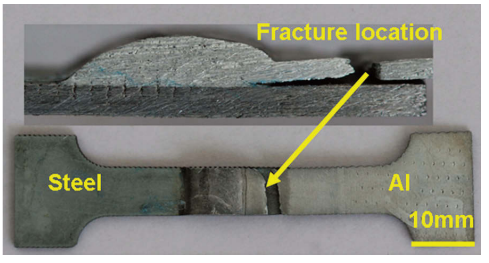

Fig. 18 — Failure location of CMT weld-braze of AA6061-T6 to galvanized boron steel at the aluminum heat-affected zone.

tion, the Zn coating was vaporized due to its low boiling point (i.e., 960°C), and the evaporation of Zn likely took away a significant amount of heat generated by the arc, and consequently, the thickness of Fe-Al IMC was reduced due to lower reaction temperature and less reaction time. Furthermore, the results shown in Ref. 27 showed that the existence of thin Fe-Al IMC between the coating layer and steel base metal during the hot-dip galvanizing process also inhibited the chemical reaction between Fe and Al and obstructed the interdiffusion between Fe and Al when joining Al to galvanized steel. However, under the same welding condition, Fe-Zn coating was not fully molten due to its high melting point, and consequently hindered the wetting of the molten filler metal on the steel substrate. As a result, welds with poor quality were produced. For CMT welding AA6061-T6 to bare boron steel, massive brittle Fe-Al IMC were formed due to the direct mixing of molten filler metal and molten steel, and the cracks likely originated from the reaction layer and propagated along the weld metal due to thermal residual stresses after welding. For CMT welding AA6061-T6 to Al-Si-coated boron steel, a large amount of Fe-Al IMC were produced due to the existence of 35-mm-thick Fe-Al IMC layer on the coating and lo-

Table 8 — EDS Results of Zones 1–7 in Fig. 13

Location	Al (at.-%)	Si (at.-%)	Fe (at.-%)	Zn (at.-%)	Possible Phase
1	22.5	4	73.5	0	Fe_3Al
2	69.7	14.4	15.9	0	$FeAl_3$
3	20.9	1.2	61.8	16.1	Fe_2Al_5 + Fe_4Al_{13} + α-Al + α-Zn
4	34.3	2	57.9	5.8	Rich-zinc Fe-Al IMC
5	94.9	1.1	2.5	1.5	Rich-zinc α-A1
6	0	0	13.2	86.8	$FeZn_{10}$
7	0	0	13.7	86.3	$FeZn_{10}$

Table 9 — EDS Results of Zones 1–5 in Fig. 15

Location	Al (at.-%)	Si (at.-%)	Fe (at.-%)	Zn (at.-%)	O (a.- %)	Possible Phase
1	70.3	2	0	22.4	0	Al-Zn eutectoid
2	92.6	1.8	0	5.6	0	α-Al
3	1.6	98.3	0	0.1	0	Si granule
4	70.5	1.8	27.7	0	0	Fe_4Al_{13}
5	72.2	3.9	23.9	0	0	$FeAl_3$ + Fe_2Al_5

cally molten steel base metal, and the load-bearing capability of the welded-brazed joints decreased drastically, which easily led to the detachment between the weld metal and base Al-Si boron steel under thermal-induced residual stresses.

Conclusions

1) The effect of coating on CMT joining of AA6061-T6 to boron steel has been investigated. It was found that a zinc coating on the steel substrate is essential. Pure Zn coating on galvanized boron steel was molten under the arc, and it enhanced the wetting of molten aluminum filler metal onto the solid steel substrate. Consequently, welds with a smooth appearance and low reinforcement were produced.

2) Fe-Zn coating from galvannealed boron steel was barely molten under the arc due to its high melting point, and consequently it barely enhanced the molten aluminum filler metal to wet the steel substrate. As a result, welds with poor quality were produced.

3) During CMT joining AA6061-T6 galvanized boron steel, element zinc was evaporated. The heat dissipation from the evaporation of the Zn reduced the temperature of the weld pool, and consequently decreased the growth of brittle Fe-Al intermetallics between the aluminum weld metal and the steel substrate.

4) Sound AA6061-T6-bare boron steel and AA6061-T6-Al-Si-coated boron steel joints could not be produced by CMT arc welding technique due to a large formation of the brittle $FeAl_3$ intermetallic during the welding process.

Acknowledgments

This work was financially supported by National Nature Science Foundation of China (No. 51265028) and GM Global Research and Development Center.

References

1. Karbasian, H., and Tekkaya, A. E. 2010. A review on hot stamping. *Journal of Materials Processing Technology* 210 (15): 2103–2118.

2. Miller, W. S., Zhuang, L., and Bottema, J. 2000. Recent development in aluminum alloys for the automotive industry. *Materials Science and Engineering* A 280: 37–49.

3. Gould, J. E. 2012. Joining aluminum Sheet in the automotive industry — A 30 Year history. *Welding Journal* 91(1): 23–34.

4. Naderia, M., Ketabchi, M., Abbasi, M., and Bleck, W. 2011. Analysis of microstructure and mechanical properties of different high strength carbon steels after hot stamping. *Journal of Materials Processing Technology* 211: 1117–1125.

5. Lorenz, D., and Roll, K. 2005. Modelling and analysis of integrated hot forming and quenching processes. *Proc. Sheet Metal 2005 Conf.*, pp. 787–794.

6. Dong, H. G. 2012. Dissimilar metal joining of aluminum alloy to galvanized steel with Al-Si, Al-Cu, Al-Si-Cu and Zn-Al filler wires. *Journal of Materials Processing Tech* 212: 458–464.

7. Lee, J. K., Kumai, S., Kawamura, N., Ishikawa, N., and Furuya, K. 2007. Growth manner of intermetallic compounds at the weld interface of steel/aluminum alloy lap joint fabricated by a defocused laser beam. *Materials Transaction* 48: 1396–1405.

8. Travessa, D., Ferrante, M., and Ouden, G. 2002. Diffusion bonding of aluminum oxide to stainless steel using stress relief interlayers. *Materials Science and Engineering A* 337: 287–296.

9. Acarer, M., and Demir, B. 2008. An investigation of mechanical and metallurgical properties of explosive welded aluminum-dual phase steel. *Materials Letters* 62(25): 4158–4160.

10. Taban, E., Gould, J. E., and Lippold, J. C. 2010. Dissimilar friction welding of 6061-T6 aluminum and AISI steel: Properties and microstructural characterization. *Materials and Design* 31: 2305–2311.

11. Fukumoto, S., Tsubakino, H., Okita, K., Aritosh, M.I., and Tomita, T. 1999. Friction welding process of 5052 aluminium alloy to 304 stainless. *Material Science Technology* 15(9): 1080–1086.

12. Taban, E., Gould, J. E., and Lippold, J. C. 2010. Characterization of 6061-T6 aluminum alloy to AISI steel interfaces during joining and thermo-mechanical conditioning. *Materials Science and Engineering A* 527: 1704–1708.

13. Tsujino, J., Hidai, K., Hasegawa, A., Kanai, R., Matsuura, H., Matsushima, K., and Ueoka, T. 2002. Ultrasonic butt welding of aluminum, aluminum alloy and stainless steel plate specimens. *Ultrasonic* 40: 371–374.

14. Zhang, H. T., Feng, J. C., He, P., Zhang, B. B., Chen, J. M., and Wang, L. 2009. The arc characteristics and metal transfer behavior of cold metal transfer and its use in joining aluminum to zinc-coated steel. *Materials Science and Engineering A* 499: 111–113.

15. Cao, R., Yu, G., Chen, J. H., and Wang, P. C. 2013. Cold metal transfer joining aluminum alloys to galvanized mild steel. *Journal of Materials Processing Technology* 213: 1753–1763.

16. Song, J. L., Lin, S. B., Yang, C. L., and Fan, C. L. 2009. Effects of Si additions on intermetallic compound layer of aluminum-steel TIG welding-brazing joint. *Journal of Alloys and Compounds* 488: 217–222.

17. Peyre, P., Sierra, G., and Deschaux, B. F. 2007. Generation of aluminum–steel joints with laser-induced reactive wetting. *Materials Science and Engineering A* 444: 327–338.

18. Yang, X. R. 2006. Cold metal transfer MIG/MAG dip-transfer process for automated applications. *Arc Welding Machine* 36: 5–7.

19. Kima, C., Kang, M. J., and Park, Y. D. 2011. Laser welding of Al-Si coated hot stamping steel. Procedia Engineering 10: 2226–2231.

20. Cao, R., Wen, B. F., Chen, J. H., and Wang, P. C. 2013. Cold metal transfer joining of magnesium AZ31B-to-aluminum A6061-T6. *Materials Science and Engineering A* 560: 256–266.

21. Pickin, C. G., Williams, S. W., and Lunt, M. 2011. Characterization of the cold metal transfer (CMT) process and its application for low dilution cladding. Journal of *Materials Processing Technology* 211: 496–502.

22. Alloy Phase Diagram Database™. ASM International.

23. Li, Z., Su, X. P., He, Y. H., Tan, Z., and Yin, F. C. 2008. Growth of intermetallic compounds in solid Zn/Fe and Zn/Fe-Si diffusion couples. *The Chinese Journal of Nonferrous Metals* 18: 1639–1644.

24. Li, L. Q., Tan, C. W., Chen, Y. B., and Guo, W. 2012. Influence of Zn coating on interface reactions and mechanical properties during laser welding-brazing of Mg to steel. *Metallurgical and Materials Transactions* 43A: 4740–4754.

25. Eustathopoulos, N., Michael G. N., and Drevet, B. 1999. *Wettability at High Temperatures*. Department of Materials Science and Metallurgy. University of Cambridge, UK.

26. Ghiotti, A., Bruschi, S., and Borsetto, F. 2011. Tribological characteristics of high strength steel sheets under hot stamping conditions. *Journal of Materials Processing Technology* 211: 1694–1700.

27. Murray, J. L. 1986. Massalski T. B. (ed.) *Binary Alloy Phase Diagrams*. ASM International, Materials Park, Ohio, p. 185.

28. Agudo, L., and Eyidi, D. 2007. Intermetallic Fe_xAl_y-phases in a steel/Al-alloy fusion weld. *J. Mater. Sci* 42: 4205–4214.

29. Kato, T., Nunome, K., Kaneko, K., and Saka, H. 2000. Formation of ζ phase at an interface between an Fe substrate and a molten 0.2 mass % Al-Zn during galvannealing. *Acta Mater* 48: 2257.

30. Abea, Y., Katob, T., and Moria, K. 2009. Self-piercing riveting of high tensile strength steel and aluminum alloy sheets using conventional rivet and die. *Journal of Materials Processing Technology* 209(8): 3914–3922.